Batteries & Supercaps

Research Article
doi.org/10.1002/batt.202500284

Chemistry Europe
European Chemical Societies Publishing

www.batteries-supercaps.org

Electrochemical Impedance Spectroscopy-Based Diagnosis of Cell Imbalances in Series-Connected Battery Modules

Sehriban Celik, Zhan Ma,* Zijuan Hong, Alexander Blömeke, David Wasylowski, and Dirk Uwe Sauer

Effective battery management systems are essential for battery energy storage systems (BESSs), particularly for managing inhomogeneities among series-connected cells requiring sophisticated diagnostic methods. Although electrochemical impedance spectroscopy (EIS) is a recognized diagnostic tool, its application has been mainly limited to individual cells. This limitation restricts the ability to diagnose the performance of entire battery modules. By extending application of EIS to the module level, this study provides a more comprehensive perspective on battery diagnostics. Reflecting real-world challenges for battery modules, it focuses on modules with series-connected cells under varying conditions. It encompasses two scenarios: state of charge (SOC) and state of health (SOH) imbalances. The module-level EIS measurements are analyzed by extending the commonly used single-point impedance diagnostic with two novel approaches: Pearson correlation analysis and support vector machine (SVM) classification. The findings show that while single-point impedance diagnostic has limitations in complex sample pools, Pearson correlation analysis and SVM classification are more effective methods that provide promising results in detecting and understanding cell imbalances. This study provides insights into the impact of cell SOC and SOH imbalances on the module's EIS, and it demonstrates the potential of advanced analytical techniques to improve the diagnostics of battery modules in BESSs.

1. Introduction

Batteries play an essential role in enhancing global energy efficiency and reducing reliance on fossil fuels. In electric vehicles (EVs) and other storage applications, batteries are expected to significantly contribute to achieving the CO_2 emission reductions necessary to meet net-zero emission goals worldwide. The International Energy Agency (IEA) forecasts a steady increase in the use of batteries within the global automotive and power industries.[1]

The reliability of batteries is closely linked to the efficiency of their management systems. Therefore, monitoring the battery states, such as state of charge (SOC) and state of health (SOH), is essential for optimal performance.[2] As most applications use lithium-ion batteries due to their high energy density and efficiency, integrating these batteries introduces new safety challenges, particularly regarding intercell imbalances within battery modules. Such imbalances can lead to deviating cell voltages over time, exposing batteries to overvoltage conditions that result in premature cell degradation, safety risks, including explosion hazards, and reduced capacity due to early charge and discharge termination.[3] To address these challenges, effective battery management systems (BMSs) must incorporate advanced diagnostic methods.

Electrochemical impedance spectroscopy (EIS) has emerged as a critical battery diagnostic method in this context because of its comprehensive information yield. EIS enhances the understanding of battery conditions by applying a small-amplitude current or potential perturbation to excite batteries at various frequencies. The measured response to this perturbation allows for the calculation of a transfer function, representing the electrochemical impedance of the batteries.[4] This technique reveals a strong correlation between impedance and battery conditions, such as temperature, SOC, and SOH.[5–16] Although EIS has traditionally been used to analyze the electrochemical characteristics of individual cells, its nondestructive nature makes it suitable for more than just cell-level analysis. In recent studies, its applications have been extended to battery modules in which battery cells are interconnected in complex configurations in EVs and stationary

S. Celik, Z. Ma, Z. Hong, A. Blömeke, D. Wasylowski, D. U. Sauer
Chair for Electrochemical Energy Conversion and Storage Systems
Institute for Power Electronics and Electrical Drives (ISEA)
RWTH Aachen University
Campus-Boulevard 89, 52074 Aachen, Germany
E-mail: zhan.ma@isea.rwth-aachen.de, batteries@isea.rwth-aachen.de

S. Celik, Z. Ma, Z. Hong, A. Blömeke, D. Wasylowski, D. U. Sauer
Center for Ageing, Reliability and Lifetime Prediction of Electrochemical and Power Electronic Systems (CARL)
RWTH Aachen University
Campus-Boulevard 89, 52074 Aachen, Germany

S. Celik, Z. Ma, Z. Hong, A. Blömeke, D. Wasylowski, D. U. Sauer
Juelich Aachen Research Alliance
JARA-Energy
Templergraben 55, 52056 Aachen, Germany

D. U. Sauer
Helmholtz Institute Münster (HI MS)
IMD-4 - Forschungszentrum Jülich
52425 Jülich, Germany

Supporting information for this article is available on the WWW under https://doi.org/10.1002/batt.202500284

storage system applications to provide valuable information about battery module performance. These studies primarily delve into three main categories, which are outlined below.

Category I: EIS measurement and analysis are conducted on different battery module configurations in the first-type category. Rüther et al.[17] demonstrated EIS's effectiveness in detecting inhomogeneities in series-connected lithium-ion battery packs. Their analysis is based on impedance data collected from cells, and features derived from the imaginary part of the impedance are found to be particularly well-suited for detecting inhomogeneities. Ank et al.[18] used the galvanostatic EIS method on different multicell topologies to detect defects. Yokoshima et al.[19] introduced square-current EIS as a simple approach for measuring impedance in large-scale lithium-ion battery systems. Kasper et al.[20] implemented EIS analysis using a battery charger and DC–DC converters, with applications at both the cell and small-scale pack levels. Recently, Zhang et al.[21] proposed a module-level EIS method for lithium plating diagnosis using an equivalent sampling method and a perturbation structure for the in situ EIS perturbation generation.

In addition to detecting performance issues, EIS was used to assess aging and second-life applications of battery modules. Kehl et al.[22] demonstrated that EIS is more adept at detecting subtle differences between aged modules than existing current interrupt (CI) analysis and capacity testing and that it reliably identifies robust aged modules for second-life applications. Wang et al.[23] proposed a rapid regrouping strategy using EIS and short-term dynamic voltage to analyze and improve the consistency and SOH of cells in retired battery packs for second-life applications. Li et al.[24] evaluated the fading characteristics of retired EV battery modules using EIS and explored their application in photovoltaic power plants for second-life energy storage applications. However, these studies did not focus on the potential of using module-level EIS to detect internal cell imbalance.

Category II: Studies in this category prove EIS's potential in detecting inconsistencies within modules with parallel-connected cells. Zhang et al.[25] showed EIS's potential in estimating SOH and detecting inconsistencies in parallel-connected modules. Yang et al.[26] investigated the influence of connection impedance on the performance of parallel-connected lithium-ion battery modules and diagnosed faulty electrical contact points using EIS. However, these two studies used EIS data from modules with parallel-connected cells. Internal imbalance detection for modules with series-connected cells using module-level EIS has not yet been thoroughly researched.

Category III: Togasaki et al.[27] proposed a method of single-frequency EIS whereby EIS is performed at a predetermined frequency to detect SOC imbalances in battery modules, thus preventing overcharging and overdischarging. Nevertheless, the analysis method is limited to the observation of Nyquist or Bode plots, which possibly ignore potential correlations between the impedance and the internal imbalance.

Diverging from these studies, the main objective of this work is to detect internal imbalances in SOC and SOH within battery modules that contain series-connected cells using module-level EIS measurements. This paper then aims to improve the analysis methods on module-level EIS by comparing three methods: single-point impedance diagnostic, an advanced statistical approach of the Pearson correlation analysis, and an advanced machine learning (ML) model of support vector machine (SVM) classification. The focus is on the effectiveness of the methods in detecting and analyzing internal imbalances within the battery modules.

Regarding the above three battery diagnostic methods for EIS, the single-point impedance diagnostic has proven to be a powerful tool for assessing battery states by extracting specific frequency points from a broader EIS measurement frequency range. This method identifies key single-frequency points that correlate with various states of the battery. Several studies have validated its effectiveness for detailed battery condition analysis, including SOH evaluation,[28,29] defect detection,[30] temperature distribution estimation,[31,32] and fault identification.[33] The Pearson correlation analysis method goes beyond single-point impedance diagnostic by examining the relationship between impedance characteristics and battery states. This method has been used as a feature selection method in estimating the SOC and SOH of lithium-ion batteries.[34–36] Another method of analyzing and classifying EIS data for battery diagnostics encompasses the application of ML models, especially SVM. SVM is a widely used supervised ML model in classification and pattern recognition tasks. Its operational mechanism identifies an ideal hyperplane that effectively distinguishes data points from different classes in a projected n-dimensional space.[37,38] Compared to other ML approaches, SVM is particularly useful for EIS data, as it can overcome nonlinear difficulties by transforming nonlinear problems in lower dimensions into linear problems in higher dimensions, especially when there are nonlinear correlations between variables.[39] Predicting the SOC and SOH of lithium-ion batteries is highly dependent on this transformation, as SVM plays a vital role in ensuring accurate and reliable modeling.[39,40] Furthermore, the application of SVM with a linear kernel function has shown potential in accurately identifying hyperplanes to effectively separate nonlinear datasets and maximize the distance between support vectors.[37]

By comparing these analytical techniques, this study comprehensively evaluates their effectiveness in detecting SOC and SOH imbalances in battery modules composed of series-connected cells using module-level EIS measurements. "Experimental Section" provides the specifications of the battery modules and devices used, as well as detailed measurement scenarios and procedures applied during the experiments. Section "Analytical Methods for Module-Level EIS Data" focuses on analyzing the results of module-level EIS measurements using the above three methods. Section "Results and Discussion" presents experimental findings and the analysis, interpretation, and comparison of the results using three analytical methods. Finally, the "Conclusion"

section summarizes the main findings of this research and highlights the practical applications of the methodologies employed for module-level EIS.

2. Experimental Section

2.1. Battery Modules

The impedance measurements were carried out on three battery modules, each with three different cells connected in series. The modules were arranged systematically to investigate the influence of the SOC and SOH imbalances on their overall impedance. **Table 1** shows the SOH of the cells inside each module and the effective SOH of all the modules.

Module-1 (fresh module) was assembled using three fresh cells. In contrast, Module-2 (aged module) was constructed with three aged cells that were cycled under varied depth of discharge (DOD). Module-3 (mixed module) consists of a single aged cell and two new cells, which allows the observation of SOH imbalance within a module. These cell combinations were developed to understand real-world scenarios where batteries have different SOH levels due to different usage conditions and aging factors.

EIS measurements were performed at the module level to investigate the influence of SOC and SOH imbalances on the impedance characteristics of cells and modules. The performance of the modules comprising cells with varying SOH will be influenced by the weakest cell, as they are connected in series. In the case of Module-3, despite having two cells with an SOH of 100%, the presence of a cell with an SOH of 88.24% may constrain the overall performance of the module. Consequently, the module's SOH was considered to be 88.24%. Nevertheless, the exact influence on the module's performance may differ based on the specific setup and design.

Table 1. SOH of the three modules, each with the three series-connected cells.

Module	Cell-1 SOH [%]	Cell-2 SOH [%]	Cell-3 SOH [%]	Module SOH [%]
1	100%	100%	100%	100%
2	90.88%	90.58%	88.24%	88.24%
3	100%	100%	88.24%	88.24%

2.2. Experimental Setup

Commercial cylindrical lithium-ion battery cells, specifically Samsung SDI INR18650-35 E with a capacity of 3400 mAh, were used for this investigation. These cells feature a lithium–nickel–cobalt–aluminum oxide (LiNiCoAlO2, abbreviated as NCA) cathode and graphite (wt. 1% silicon) anode.

The Digatron MCT ME battery cycler was used for charging and discharging at the cell level, while a Digatron BNT ME battery cycler was used for charging and discharging at the module level. EIS measurements were conducted via the Digatron EIS-Meter. This instrument measures the batteries' impedance using the single-sine EIS method. It autonomously modulates the amplitude of the current delivered to the battery, resulting in a battery voltage response with an amplitude of 10 mV (quasi-galvanostatic mode). Furthermore, it has a direct current (DC) voltage range of 0–20 V and an alternating current (AC) output of 2 A (peak-to-peak). Therefore, it enables the measurement of impedance at both the individual cell and module levels. All measurements were carried out at a stable temperature of 25 °C within a Weiss Technik LabEvent temperature chamber. The whole experimental setup is illustrated in Figure S1. A dedicated printed circuit board was designed for the series connection of the cells. The cell holder also ensures integration with both the cycler and EIS device channels.

2.3. Measurement Execution

The primary aim of using the three battery modules presented in the preceding section has several aspects. These include exploring the SOC or SOH imbalances within the modules and assessing the feasibility of detecting imbalances in both SOC and SOH through the module-level EIS measurements. Two scenarios shown in **Table 2** are considered to accomplish this objective.

Scenario-1 focuses on the consequences of imbalances in SOC within Module-1 and Module-2, which are relatively balanced in terms of SOH, and also includes Module-3 to investigate the influence of SOC imbalances in a battery module that is not balanced in SOH. The objective of these measurements was to investigate the impact of the SOC difference of a single cell within the modules on the EIS responses of the modules. The measurements were realized by conducting the module-level EIS

Table 2. SOC distributions in two scenarios representing low and high degrees of imbalances, quantified via the CoV.

Scenarios	Modules	Cell-1 SOC [%]	Cell-2 SOC [%]	Cell-3 SOC [%]	CoV_{SOC} [%]	CoV_{SOH} [%]
Scenario-1 (SOC Imbalanced Scenario)	Module-1/2/3	100	100	100	0.00	0.00/1.31/5.77
		100	100	80	10.10	
		100	100	50	28.28	
		100	100	20	51.43	
		100	100	5	65.54	
Scenario-2 (SOH Imbalanced Scenario)	Module-1	5-100	5-100	5-100	0.00	0.00
	Module-2	5-100	5-100	5-100	0.00	1.31
	Module-3	5-100	5-100	5-100	0.00	5.77

Research Article
doi.org/10.1002/batt.202500284
Chemistry Europe
European Chemical Societies Publishing

measurements after discharging the selected cell (Cell-3) in each module to the desired SOC level.

In Scenario-2, the objective was to examine the impact of SOH imbalances with three modules as they have different SOH levels. Module-1, the fresh module, was considered the reference control group with uniform SOH. Module-2, on the other hand, represents a uniformly aged module, and Module-3, the mixed module, comprised a combination of fresh and aged cells.

Table 2 also indicates the degree of variation of SOC and SOH among the cells within each module. The degree of SOC and SOH imbalances for each module was quantified using the coefficient of variation (CoV), which is a standardized measure of the dispersion of a distribution of probability. It is defined as the division of the standard deviation by the mean. The CoV can be used to compare variation between datasets with different mean values, and the following equations can be used to compute the CoV:

$$\begin{Bmatrix} \mu = \frac{\sum_{i=1}^{n} S_i}{n} \\ \sigma = \sqrt{\frac{\sum_{i=1}^{n} (S_i - \mu)^2}{n}} \\ \mathrm{CoV}_{\mathrm{SOC/SOH}} = \frac{\sigma}{\mu} \end{Bmatrix} \quad (1)$$

where σ represents the standard deviation, n is the number of cells in the module, μ represents the mean SOC or SOH of the battery module, and S_i stands for the SOC or SOH of the ith module. A higher CoV value indicates that the module has a greater level of relative imbalance, while a CoV closer to zero indicates a higher level of cell balance.

Based on the observed range of $\mathrm{CoV}_{\mathrm{SOC}}$ and $\mathrm{CoV}_{\mathrm{SOH}}$ values, the modules were divided into three qualitative categories to support comparative analysis.

Low SOC imbalanced: $\mathrm{CoV}_{\mathrm{SOC}} < 10\%$; moderate SOC imbalanced: $\mathrm{CoV}_{\mathrm{SOC}} \approx 10\%$–$50\%$; high SOC imbalanced: $\mathrm{CoV}_{\mathrm{SOC}} > 50\%$; low SOH imbalanced: CoVSOH $< 2\%$; moderate SOH imbalanced: $\mathrm{CoV}_{\mathrm{SOH}} \approx 2\%$–$6\%$; high SOH imbalanced: $\mathrm{CoV}_{\mathrm{SOH}} > 6\%$.

These categories are not universal and reflect the empirical spread in our dataset, but they are used to distinguish imbalance levels for interpretative purposes.

Module-level EIS measurements were conducted for each scenario at five distinct SOCs: 100%, 80%, 50%, 20%, and 5%, respectively. The measurement methodology begins with a conditioning cycle that ends with a constant current-constant voltage (CC–CV) phase with a cutoff current of 0.02C to ensure that all modules, regardless of their aging status, reach SOC of 100%. After 1 hour of relaxation intervals, EIS measurements were performed on three modules within the frequency range spanning from 20 mHz to 2 kHz. Subsequently, in Scenario-2, referred to as the SOH imbalanced scenario, every individual cell experienced a discharge down to the specified SOC (80%, 50%, 20%, and 5%, respectively) at a rate of 0.5C. In Scenario-1, only the selected cell undergoes the same discharge process. The cells that were discharged were rested for 1 h once they reached the specified SOC. Following that, the total impedance of each module was measured. This cycle was repeated for predetermined SOC values, and the measurements were completed when the last SOC level of 5% was reached for each scenario. The module-level EIS measurement procedure is shown in Figure S2.

3. Analytical Methods for Module-Level EIS Data

3.1. Single-Point Impedance Diagnostic Method

As a feature-based impedance analysis, the single-point impedance diagnostic method is used to determine whether impedance magnitude changes occur at predetermined frequencies. Concentrating on particular frequencies within the frequency range provides an evaluation of impedance magnitude behavior, which is crucial for identifying cell imbalances within the battery modules. Within this diagnostic approach, two key frequencies are identified. One from the high-frequency range, named the Ohmic frequency (f_{ohmic}), represents the frequency point where the impedance is purely resistive. A second one from the low-frequency range, called diffusion onset frequency ($f_{\mathrm{diffusion}}$), indicates the point where diffusion processes begin in the battery, mathematically, the inflection point with the highest real part.[41] These frequencies are shown in a Nyquist plot in **Figure 1** as an example of the module-level EIS measurement result of an aged module with 88% SOH and a fresh module with 100% SOH, both at 100% SOC, over a frequency range from 20 mHz to 2 kHz. This plot also shows the three frequency ranges (high, medium, and low) considered in this research. It should be noted that while these key characteristic frequencies are commonly theoretically grounded, their absolute value may shift due to aging. Especially in the

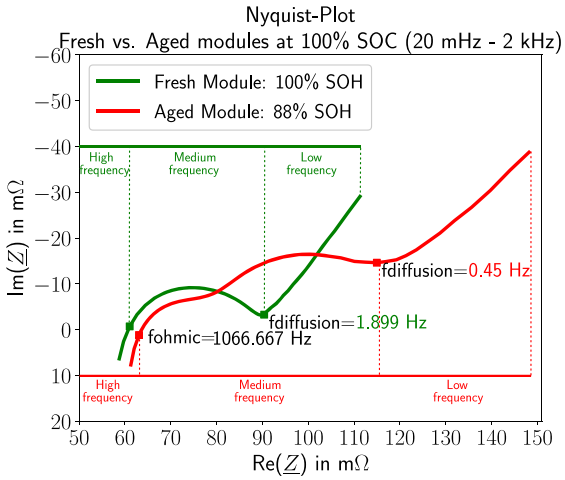

Figure 1. EIS comparison of fresh and aged modules using the single-point impedance diagnostic method. In the Nyquist diagram, the green and red EIS spectra represent the fresh and aged modules, respectively. The key frequencies determined for diagnostic purposes include the Ohmic frequency ($f_{\mathrm{ohmic}} = 1067$ Hz) in the high-frequency range, where the impedance is purely Ohmic, and the frequency of the start of diffusion ($f_{\mathrm{diffusion}}$), which is different for each module (1.899 Hz for the fresh module and 0.45 Hz for the aged module) and indicates the point at which diffusion processes begin. The frequency ranges are divided into high, medium, and low, as indicated by the dashed lines. This analysis method improves the detection of cell imbalances by focusing on the impedance magnitude behavior at these specific frequencies.

low-frequency region, degradation mechanisms such as cathode particle cracking and the formation of cathode-electrolyte interphase can alter the impedance spectrum[42] and lead to shifts in the diffusion onset frequency ($f_{diffusion}$). Therefore, these frequencies are used as reference points in this diagnostic method but are not assumed to be invariant.

3.2. Pearson Correlation Analysis

A linear correlation between the imbalance degree of battery modules (CoV_{SOC} and CoV_{SOH}) and their total impedance can be determined using the Pearson correlation coefficient (PCC), as defined in Equation (2). This statistical measure is used to identify the most relevant characteristics capable of detecting the influence of SOC and SOH imbalances on the impedance of the battery modules.

$$\rho_{X,Y} = \frac{\mathrm{E}(X,Y) - \mathrm{E}(X)\mathrm{E}(Y)}{\sqrt{\mathrm{E}(X^2) - \mathrm{E}(X)^2} \cdot \sqrt{\mathrm{E}(Y^2) - \mathrm{E}(Y)^2}} \tag{2}$$

In this study, X stands for the degree of imbalances (CoV), and Y stands for the real part (Re(Z)), imaginary part (Im(Z)), magnitude ($|Z|$ or Abs(Z)) or phase angle (θ or Pha(Z)) of the complex impedance (Z) of the modules at each frequency point. The Pearson correlation analysis first examines the linear correlations between the modules' impedance—all impedance components—and the degree of SOC imbalances (CoV_{SOC}). Secondly, the linear correlations between the modules' impedance and the degree of SOH imbalances (CoV_{SOH}) are assessed.

The strength and direction of these linear relationships are measured quantitatively by the PCC, which is between -1 and 1. A PCC value close to 1 or -1 indicates a robust positive or negative linear correlation, respectively. In contrast, a value near zero indicates no detectable correlation between two variables: X and Y.[43] Figure S3 provides a scatter plot that visually presents the linear correlation between CoV_{SOC} and the Im(Z) of a battery module at 107 Hz.

3.3. Support Vector Machine Classification

The fundamental principle of SVM involves the identification of an ideal hyperplane that effectively separates the data points belonging to distinct classes within a projected n-dimensional space, as depicted in Figure S4. In this study, SVM with a linear kernel function that enables the classification of datasets that are not linearly separable is used to classify EIS data. Each EIS measurement conducted on a module is labeled as SOC/SOH balance or SOC/SOH imbalance.

When datasets are not entirely separable, SVM uses a soft margin technique, which allows specific data points to be on the incorrect side of the hyperplane with a particular penalty.[37] Equation (3) gives the mathematical representation of this optimization problem that encompasses this approach

$$\left\{ \begin{array}{l} \min\left(\frac{1}{2}||w||^2 + C\sum_{i=1}^{n}\xi_i\right) \\ \mathrm{s.t.} y_i(w \cdot x_i + b) \geq 1 - \xi_i \\ \xi_i \geq 0, i = 1, \ldots, n \end{array} \right\} \tag{3}$$

where w (the weight factor) is the vector that represents the optimal hyperplane for separating the two groups of datasets. The vector w is the set of coefficients learned by the SVM during the training process and indicates the influence of each feature on the classification decision. The bias vector is denoted by b and $y_i \in \{1, -1\}$ is the normalized classification boundary. The slack variable ξ accounts for misclassifications and is influenced by the C parameter, which determines the amount of misclassifications that should be penalized.

The effectiveness of an SVM classification model can be evaluated using a number of metrics that provide information about the model's ability to classify modules efficiently. The confusion matrix, as given in **Table 3**, is an essential tool for the evaluation. In this table, the terms true positive (TP), false negative (FN), false positive (FP), and true negative (TN) are used to describe the model's classification results. TP means that the model correctly identified the module as a "balanced module", while FP implies that the model incorrectly identified the module as a "balanced module". Similarly, TN means that the model incorrectly identified the module as an "imbalanced module", while FN implies that the model incorrectly identified the module as an "imbalanced module".

From this confusion matrix, multiple metrics such as Precision, Recall, and F1 score can be calculated. These metrics give information about the performance of the classification model.[44,45] Precision quantifies the proportion of positive class predictions accurately classified out of all the positive predictions made. In this study, this metric quantifies the proportion of battery modules predicted as "balanced module" that were correctly classified out of all the "balanced module" predictions made by the model. Recall is related to the ratio of correctly identified positive cases relative to the overall number of instances belonging to the positive class within the specified category. Here, it indicates the proportion of correctly identified "balanced modules" in relation to the total number of balanced modules. The F1 score is a statistical measure that combines precision and recall, providing a balanced average representation. A high F1 score indicates not only that the SVM model predicts balanced modules accurately but also that it captures a large proportion of the balanced modules from the dataset. All these three metrics are described in Equation (4). The performance of the SVM model can be determined by analyzing these metrics together with the confusion matrix.

Table 3. Confusion matrix.

	Predicted positive [Balanced]	Predicted negative [Imbalanced]
Actual Positive (Balanced)	True Positive (TP)	False Negative (FN)
Actual Negative (Imbalanced)	False Positive (FP)	True Negative (TN)

Research Article
doi.org/10.1002/batt.202500284
Chemistry Europe
European Chemical Societies Publishing

$$\left\{\begin{array}{l} Precision = \dfrac{TP}{TP + FP} \\ Recall = \dfrac{TP}{TP + FN} \\ F1 = 2 \cdot \dfrac{\text{Precision} \cdot \text{Recall}}{\text{Precision} + \text{Recall}} \end{array}\right\} \quad (4)$$

4. Results and Discussion

The impedance results that are obtained from three battery modules under three different scenarios were subjected to the linear Kramers–Kronig (Lin-KK) test developed by the Karlsruhe Institute of Technology (KIT)[46] before being analyzed. While the Lin-KK test has traditionally been used in single-cell analysis, our study extends its application to module-level EIS data to evaluate the compliance of the impedance results with the linear time-invariant (LTI) criteria. The Lin-KK test can perform a fitting process with multiple RC elements and provide the residual value by comparing the resulting fit to the corresponding measurement.[47,48] The obtained EIS data of three modules show a maximum residual value of ±0.5% throughout all experiments. This result is consistent with the prescribed threshold for a valid measurement under the conditions of LTI systems.[47]

The results are given based on the two measurement scenarios and three analysis methods. Initially, the EIS of three series-connected modules (Module-1, Module-2, and Module-3) in the first scenario of Table 2, specifically focusing on SOC imbalances and combined SOC and SOH imbalances, will be presented. Next, the findings corresponding to all three modules in the second scenario, identifying SOH imbalances, will be shown. Before interpreting the results, it is important to acknowledge that the impedance contributions originating from the cell connections have been subtracted from the impedance values of the module. This adjustment was made to ensure that the measurements accurately reflect the essential characteristics of the battery cells.

4.1. Single-Point Impedance Diagnostic Method

4.1.1. Scenario-1: SOC Imbalance

The investigation of SOC imbalances in battery modules is conducted through EIS measurements and single-point impedance diagnostic method, focusing on three distinct modules: Module-1 (fresh module), Module-2 (aged module), and Module-3 (mixed module). As previously mentioned, each module consists of three cells connected in series, with one cell at a different SOC level, while the other two cells are consistently fully charged. The EIS of three modules, shown in Nyquist plots in **Figure 2** and corresponding to Scenario-1 in Table 2, shows significant differences in their response to SOC imbalances. These results are also provided in Bode plots in Figure S5.

In Module-1, the impedance analysis demonstrates minimal variance when the SOC of the selected cell is between 20% and 80% (80% ΔSOC and 20% ΔSOC), as shown in Figure 2a. This indicates that for a module consisting of newly manufactured cells from the same manufacturing batch, detecting

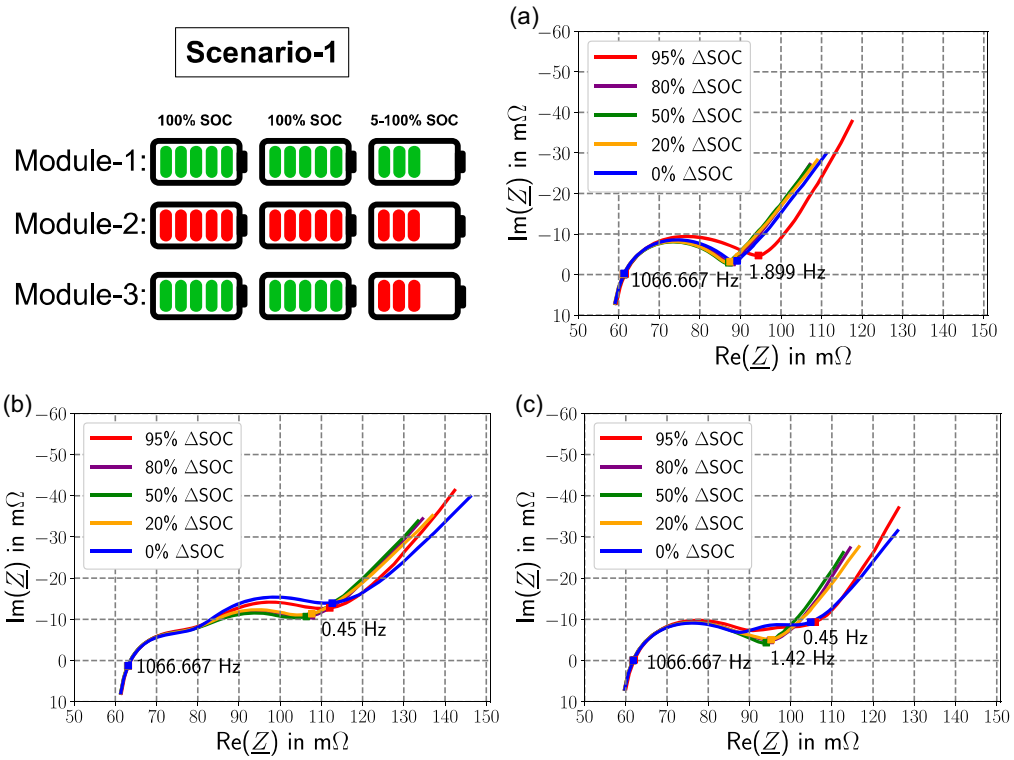

Figure 2. EIS of three modules with single-point impedance diagnostic method based on Scenario-1 of Table 2 (SOC imbalanced Scenario): a) Module-1, b) Module-2, and c) Module-3. The Ohmic (f_{ohmic}) and diffusion onset ($f_{diffusion}$) frequencies for each impedance spectrum are annotated to detect SOC imbalances in each module.

imbalances in modules is challenging due to the minor changes in impedance magnitude, even down to very low SOC levels. Findings from the literature support these observations by showing that the diameter of the semicircle in the impedance profile of a lithium-ion battery with an NCA cathode increases when the battery is discharged from 60% SOC to 0% SOC.[49] This behavior is associated with increasing charge-transfer resistance at the NCA cathode, which becomes the dominant impedance contribution at lower SOC values due to cathode reaction limitations and reduced lithium diffusion rates.[27,50] Therefore, the low-frequency impedance shifts observed in this fresh module to SOC imbalance conditions, especially in the case of 95% SOC discrepancy (95% ΔSOC) between the selected and fully charged cells, can be attributed to the electrochemical response of the selected low-SOC cell.

In contrast, Module-2, which includes aged cells with imbalanced SOC, shows a different impedance behavior. Its EIS spectra show two distinguishable semicircles at each SOC level, as shown in Figure 2b. Although the EIS spectra at ΔSOC between 20% and 80% are indistinguishable, SOC imbalances become apparent in the low-frequency range, differing from the fully charged state (0% ΔSOC). The EIS of the aged module at 95% ΔSOC resembles that of a balanced module, making detecting SOC imbalances challenging.

Similar to the results of Module-2, the EIS results of Module-3, when the selected cell is at 5% and 100% SOC, also show two semicircles, as shown in Figure 2c. On the other hand, a notable observation is the ambiguity in the EIS profile when ΔSOC changes from 80% to 20%. However, if these results are compared with the balanced state of the module (0% ΔSOC), it becomes clear that there are impedance magnitude changes in the low-frequency range.

In investigating SOC imbalances within the three modules, EIS measurements have revealed intriguing trends. Notably, Module-1, Module-2, and Module-3 show similarities in the high-frequency region, especially at f_{ohmic}, consistent over 95% ΔSOC to 0% ΔSOC at 1067 Hz. This apparent uniformity in the high-frequency range suggests that the impedance magnitude at this frequency remains relatively stable across modules in the qualitative comparison, regardless of the SOC value or aging conditions. However, the more meaningful variations in impedance are observed in the low-frequency range, especially at the diffusion onset frequency ($f_{diffusion}$) values. In particular, Module-1 shows pronounced impedance changes at 1.899 Hz, Module-2 shows different impedance characteristics at 0.45 Hz, and Module-3 shows the most significant variations at 1.42 Hz (at 80%, 50%, and 20% ΔSOC) and 0.45 Hz (at 95% ΔSOC). These variations in the low-frequency range are crucial as they emphasize the complexity of detecting SOC imbalances, especially considering the various conditions and ages of the modules.

4.1.2. Scenario-2: SOH Imbalance

The investigation into the SOH imbalanced scenario, also conducted using module-level EIS measurements, focuses on the same modules (Module-1, Module-2, and Module-3), each composed of three series-connected cells with identical SOC levels but varying SOH. Unlike the previous scenario, this scenario allows for assessing the impact of SOH imbalances within the modules on their EIS with the single-point impedance diagnostic method.

Figure 3 illustrates the comparison of EIS spectra of the three modules based on Scenario-2 of Table 2 across various SOC levels (100%, 80%, 50%, 20%, and 5%). The results are also provided in Bode plots in Figure S6. The module-level EIS measurements at all SOC values reveal that modules with aged cells (Module-2 and Module-3) exhibit a relatively high impedance magnitude in all frequency ranges compared to the SOH-balanced Module-1. Notably, the EIS of Module-1 consistently displays a single semicircle at all SOC values. In contrast, the EIS spectra of Module-2 and Module-3 at 100% and 5% SOC resemble each other and show two semicircles, as shown in Figure 3. The emergence of a second semicircle in Module-2 and Module-3 under certain conditions highlights the significant effect of the aging of the cells inside the module on the module-level EIS characteristics. Interestingly, although Module-3 exhibits a higher SOH imbalance (5.77%) than Module-2 (1.31%), the second semicircle is less pronounced in Module-3. This is attributed to the presence of three cyclic-aged NCA cells in Module-2, which are known to cause a strong impedance rise in the medium-frequency impedance region due to degradation mechanisms such as charge-transfer resistance growth, electrolyte decomposition, and structural changes in the cathode.[51,52] In contrast, the impedance contribution of the aged cell in Module-3 is partially masked by the lower impedance of two fresh cells, resulting in a less visible second semicircle despite the higher CoV_{SOH}. However, even a slight degree of SOH imbalance, as small as 1.31% in Module-2, can be detected at specific SOC levels (100% and 5%) with these module-level EIS measurements. Nevertheless, it is shown that the differences in EIS between fresh and aged modules are more pronounced than those between fresh and mixed modules.

Moreover, key frequencies (f_{ohmic} and $f_{diffusion}$) for the three modules and impedance magnitude trends for Module-2 and Module-3 compared to the balanced module (Module-1) at these frequencies can be seen in Figure 3. An increase in impedance magnitude is observed in the high-frequency region at 1067 Hz when transitioning from an SOC of 100% to 5% throughout the three modules. In the low-frequency range, the key frequencies considered are 1.899 and 0.8 Hz (from 80% SOC to 20% SOC), 1.899 and 0.45 Hz at 100% SOC, and 0.8 and 0.45 Hz at 5% SOC. At these frequencies, down to 5% SOC, Module-2 and Module-3 show an increased impedance magnitude compared to Module-1 (SOH balanced module). At 5% SOC, Module-2 still shows a higher impedance magnitude than Module-1, whereas Module-3 exhibits a lower impedance magnitude than Module-1.

Unlike the observations in Scenario-1, the impedance of the modules in this scenario exhibits changes at the considered frequency in both high-frequency and low-frequency ranges. These frequencies, particularly $f_{diffusion}$, are crucial in differentiating between balanced and imbalanced modules at 100% and 5% SOC. The observed impedance changes at the considered frequencies

Research Article
doi.org/10.1002/batt.202500284
Chemistry Europe
European Chemical Societies Publishing

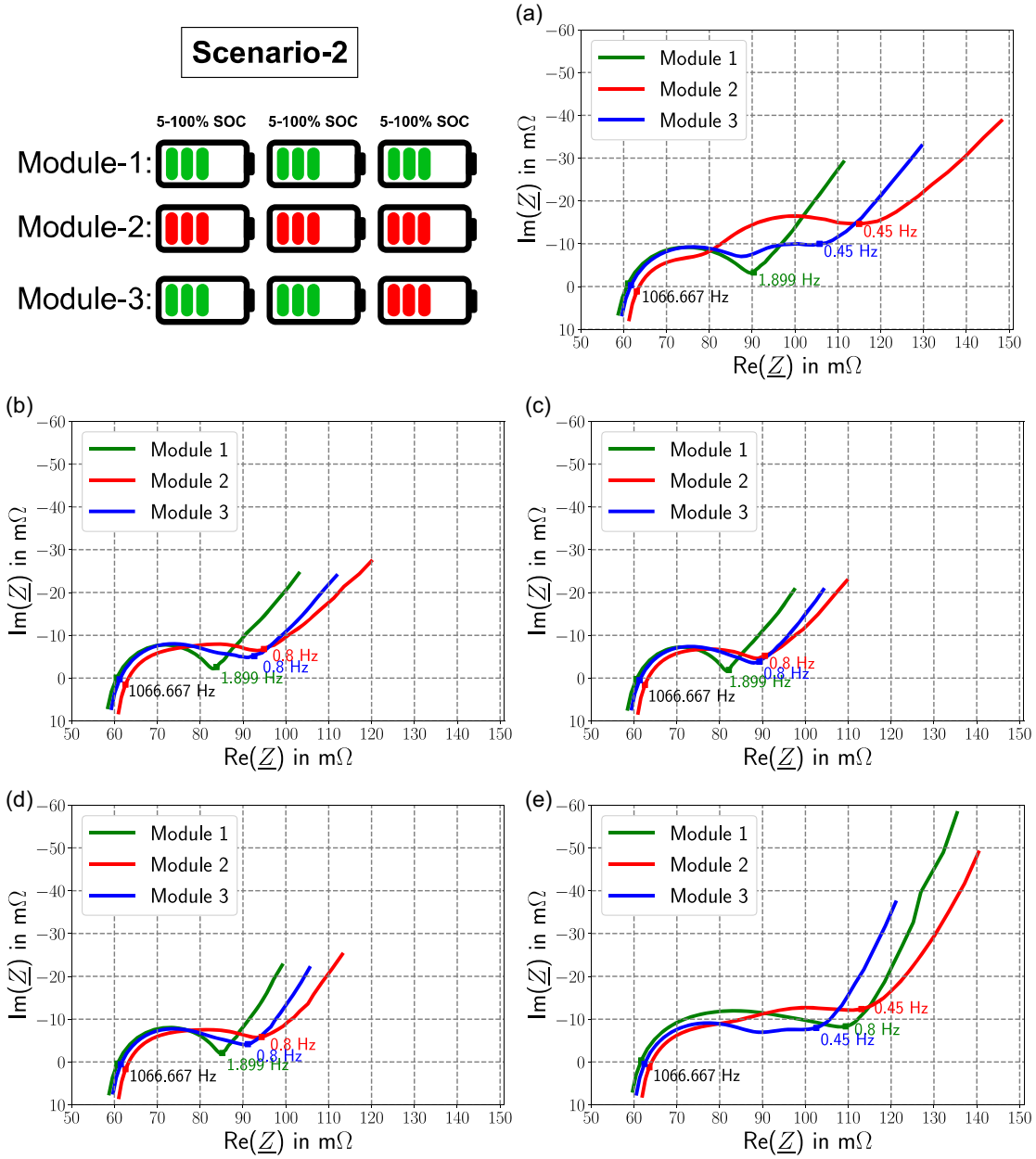

Figure 3. EIS of three modules with single-point impedance diagnostic method based on Scenario-2 of Table 2 (SOH imbalanced Modules): a) 100% SOC, b) 80% SOC, c) 50% SOC, d) 20% SOC, and e) 5% SOC. The Ohmic (f_{ohmic}) and diffusion onset ($f_{diffusion}$) frequencies are annotated to detect SOH imbalances in the modules at different SOC levels.

confirm the impedance differences and emphasize the importance of single-point impedance diagnostics for detecting and understanding SOH imbalances in battery modules.

An important finding from all these measurements is that only some frequencies consistently provide comprehensive information about impedance changes due to SOC and SOH imbalances within the modules. In addition, it is difficult to ascertain whether the impedance's real or imaginary parts change linearly or nonlinearly at these frequencies. Therefore, the Pearson correlation analysis method is employed in the following subsection to determine the frequencies that exhibit a linear correlation between the total impedance and the modules' respective degrees of imbalances for each scenario.

4.2. Pearson Correlation Analysis

4.2.1. Scenario-1: SOC Imbalance

The SOC imbalance in the three modules is examined by the Pearson correlation analysis. **Figure 4**(a) (Module-1), Figure 4(b) (Module-2), and Figure 4(c) (Module-3) show the correlation between the impedance of the modules and the degree of SOC imbalances (CoV_{SOC}) with PCCs. These results demonstrate a broader frequency range compared to previous qualitative single-point impedance diagnostic results. For Module-1, positive linear correlations between CoV_{SOC} and Re(Z), Im(Z), and Pha(Z) are observed at high frequencies, with Im(Z) showing a higher

Research Article
doi.org/10.1002/batt.202500284
Chemistry Europe
European Chemical Societies Publishing

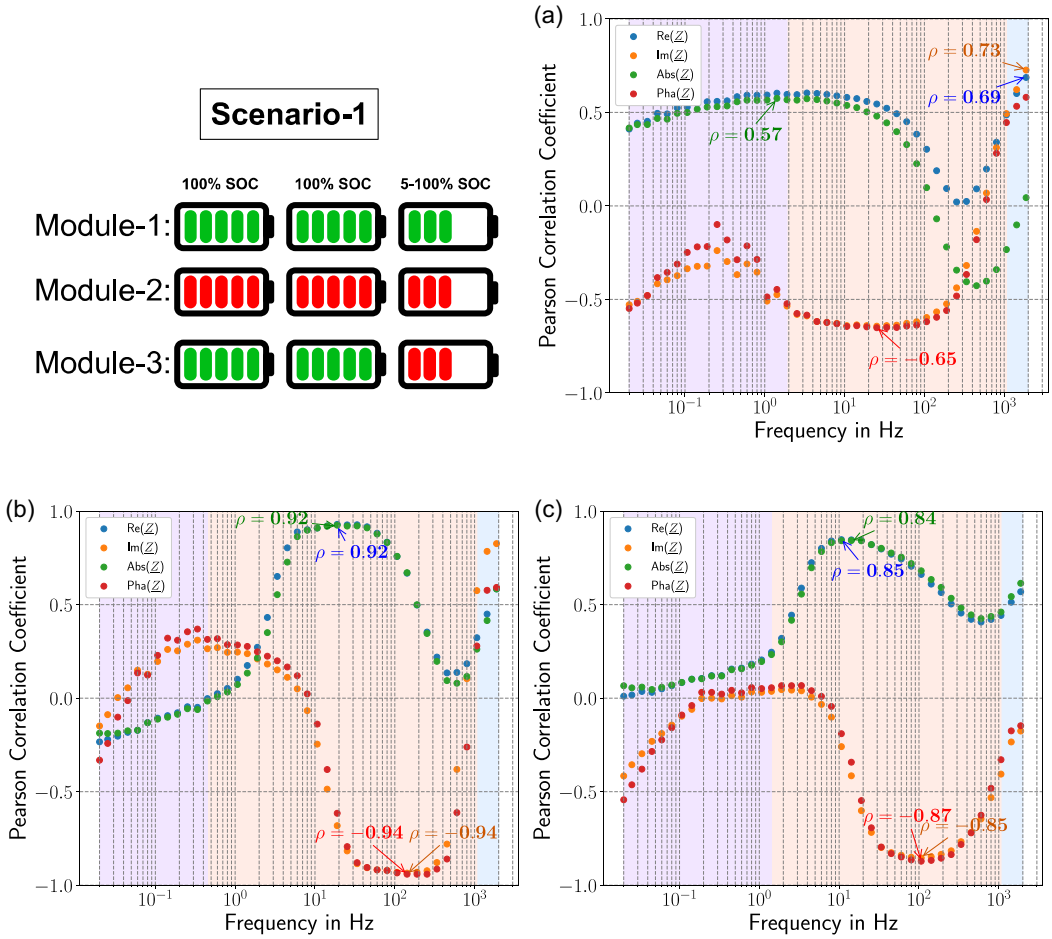

Figure 4. The correlation between the impedance of a) Module-1, b) Module-2, and c) Module-3 versus corresponding CoV_{SOC} based on Scenario-1. The shaded frequency ranges correspond to regions defined based on f_{ohmic} and $f_{diffusion}$ values in Figure 2: low frequency (purple), medium frequency (red), and high frequency (blue). Frequency ranges are module specific. The highest PCCs for each impedance parameter are annotated to detect SOC imbalances in each module.

PCC value. This trend indicates a consistent increase in these impedance parameters with an increased degree of SOC imbalances. Although high-frequency impedance appeared relatively stable in the single-point impedance diagnostic analysis, the Pearson correlation reveals consistent linear trends that are not easily detectable by qualitative analysis alone. In addition, there is a positive correlation between CoV_{SOC} and Re(Z) or Abs(Z) and a negative correlation between CoV_{SOC} and Im(Z) or Pha(Z) at the low- and medium-frequency ranges. The PCC values for Module-2 in Figure 4(b) reveal that the Re(Z) and Abs(Z) positively correlate with CoV_{SOC}, particularly in the medium-frequency range. However, the Im(Z) and Pha(Z) show both positive and negative correlations with CoV_{SOC} in the same frequency range. Module-3 shows similar trends to Module-2, with the Re(Z) and Abs(Z) predominantly positively correlated with CoV_{SOC} in the medium-frequency range. In comparison, the Im(Z) and Pha(Z) are mostly negatively correlated with CoV_{SOC}.

This consistency across frequencies for each module suggests that these ranges can be essential for detecting SOC imbalances. The identified frequency ranges that provide the highest PCC values for each module, which are consistent with the CoV_{SOC}, are also presented in Figure 4. Module-2 has higher absolute PCC values compared to Module-1 and Module-3. Moreover, the most important frequency range for Module-1 is the high-frequency range, while the medium-frequency range is significant for Module-2 and Module-3.

4.2.2. Scenario-2: SOH Imbalance

The analysis of the SOH imbalances with the same Pearson correlation methodology shifts the focus to examining how variations in the degree of SOH imbalance influence the impedance characteristics of the battery modules. The correlations of Re(Z), Im(Z), Abs(Z), and Pha(Z) with CoV_{SOH} at different SOC levels are presented in **Figure 5**. All the figures in Figure 5 show that the correlation of Re(Z) with CoV_{SOH} is positive down to 5% SOC. This indicates a consistent increase in Re(Z) with an increased degree of SOH imbalances. On the other hand, there is a negative correlation between Abs(Z) and CoV_{SOH} at all SOC levels. Im(Z) and Pha(Z) show similar trends with CoV_{SOH} at all SOCs. Down to

Research Article
doi.org/10.1002/batt.202500284

Chemistry Europe
European Chemical Societies Publishing

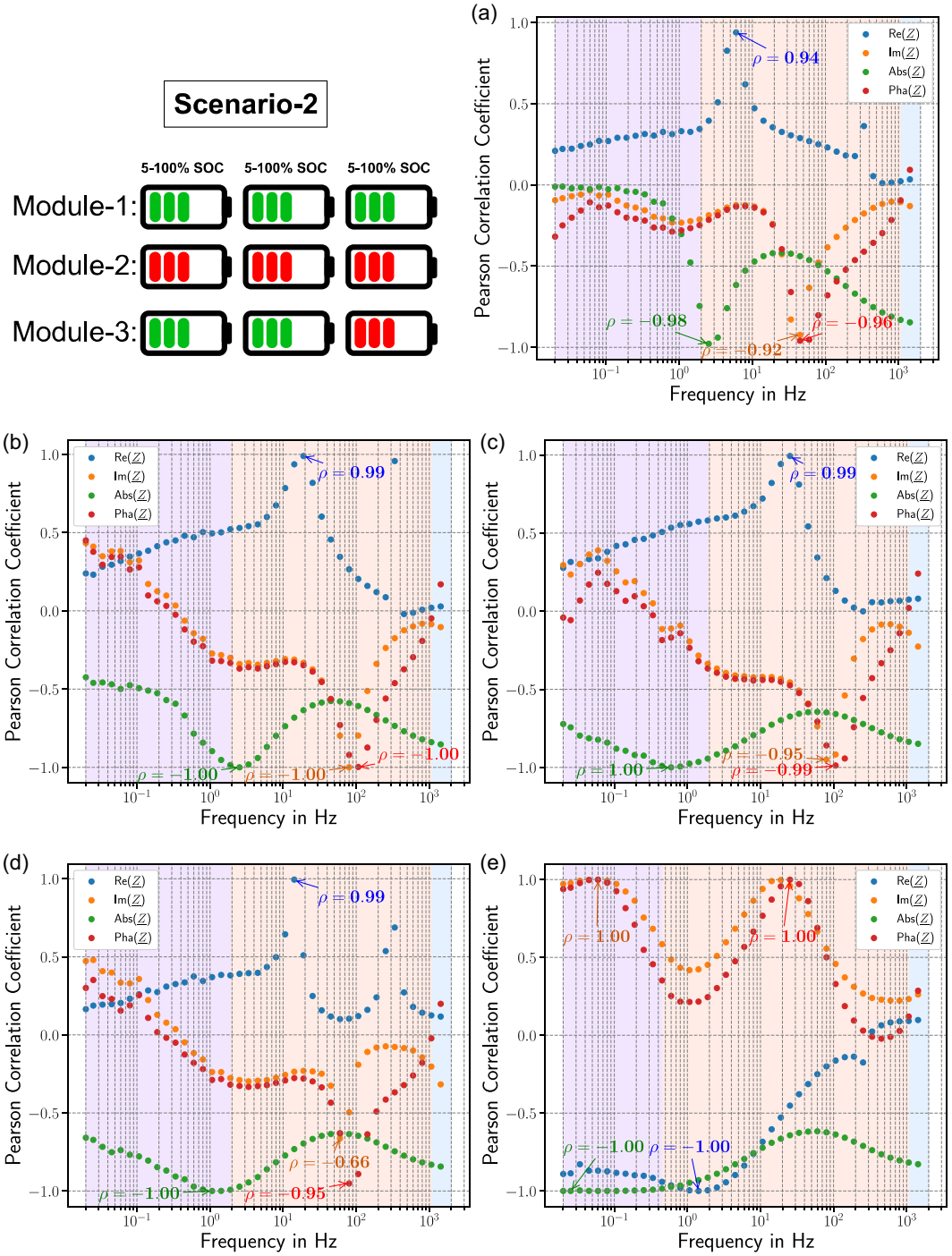

Figure 5. The correlation between the impedance of three modules versus CoV_{SOH} based on Scenario-2 a) at 100% SOC, b) at 80% SOC, c) at 50% SOC, d) at 20% SOC, and e) at 5% SOC. The shaded frequency ranges correspond to regions defined based on f_{ohmic} and $f_{diffusion}$ values in Figure 3: low frequency (purple), medium frequency (red), and high frequency (blue). The highest PCCs for each impedance parameter are annotated to detect SOH imbalances in the modules at different SOC levels.

5% SOC, Im(Z) and Pha(Z) are mostly negatively correlated, while at 5% SOC, they are positively correlated with CoV_{SOH} in all frequency ranges. A common feature of these impedance characteristics is that Re(Z) and Abs(Z) exhibit a very high linear negative correlation, essentially in the low-frequency range at 5% SOC. Conversely, Im(Z) and Pha(Z) demonstrate a high linear positive correlation in the same frequency range and SOC level. Based on these observations, the most informative condition for detecting SOH imbalances using the Pearson correlation analysis is at 5% SOC, where the strongest correlations between impedance and CoV_{SOH} occur for all impedance components, particularly in the medium- and low-frequency ranges.

Research Article
doi.org/10.1002/batt.202500284
Chemistry Europe
European Chemical Societies Publishing

4.3. Support Vector Machine Classification

4.3.1. Scenario-1: SOC Imbalance

Module-level EIS measurement data from Scenario-1 are analyzed using SVM classification with a linear kernel, where the gamma parameter is set to "scale" and the regularization parameter C is configured to a value of 1.0 to understand SOC imbalances. These measurements are labeled as "SOC Imbalance," while those from Scenario-2 are labeled "SOC Balance." The dataset is systematically split into a training set (65% of data) and a test set (35% of data), shuffled with a fixed random state to ensure consistency and reproducibility. Once the model is trained, it is evaluated using the test dataset. The precision, recall, and F1 score metrics are used to assess the model's performance during both the testing and validation phases.

The classification of SOC imbalances is performed within each module using Re(Z), Im(Z), Abs(Z), and Pha(Z) as features. As demonstrated in **Table 4**, the classification of SOC imbalances within Module-1 proved to be challenging, particularly when the Abs(Z) is used as a feature, as reflected by a low recall and an F1 score below the threshold of 0.5. This result aligns with our earlier findings that SOC imbalances cause only minor impedance variations in this module, which may be insufficient for the SVM model to distinguish between balanced and imbalanced states reliably. In contrast, the SVM classification model performs well in predicting the SOC imbalances of the other two modules, achieving a 100% accuracy for Module-3. A comparative analysis of Re(Z), Im(Z), Abs(Z), and Pha(Z) as features shows that Re(Z) and Im(Z) give a higher precision compared to Abs(Z), and Pha(Z) when data from all modules are consolidated. This highlights the potential benefits of using Re(Z) and Im(Z) in certain diagnostic contexts.

Table 4. SVM classification results of the SOC imbalanced scenario based on impedance parameters.

Scenario	Modules	Precision	Recall	F1 score
Scenario-1 (SOC Imbalanced Scenario)		Re(Z)		
	1	0.89	0.83	0.84
	2	0.89	0.83	0.84
	3	1.00	1.00	1.00
	1,2,3	0.85	0.72	0.73
		Im(Z)		
	1	0.80	0.50	0.46
	2	0.89	0.83	0.84
	3	1.00	1.00	1.00
	1,2,3	0.92	0.89	0.89
		Abs(Z)		
	1	0.11	0.33	0.17
	2	1.00	1.00	1.00
	3	1.00	1.00	1.00
	1,2,3	0.59	0.61	0.60
		Pha(Z)		
	1	0.80	0.50	0.46
	2	1.00	1.00	1.00
	3	1.00	1.00	1.00
	1,2,3	0.77	0.78	0.76

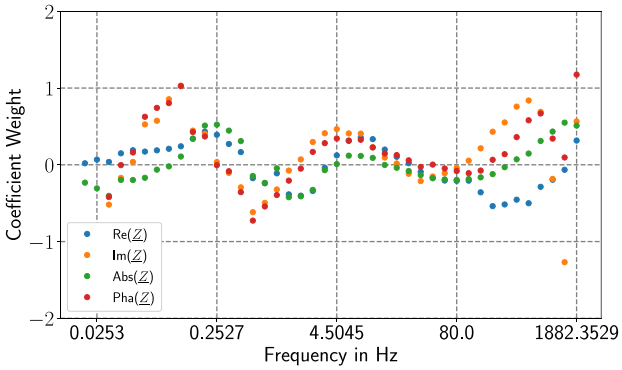

Figure 6. Coefficient weights of three modules based on Scenario-1 using Re(Z), Im(Z), Abs(Z), or Pha(Z) as a feature.

Significant coefficient weights for SOC imbalances are shown in **Figure 6**, where each point on the graph represents a coefficient weight (the elements of the weight vector w) assigned by the SVM model when the Re(Z), Im(Z), Abs(Z), or Pha(Z) is used as a feature. This visual representation identifies the frequencies that have the most significant impact on classification decisions, with distinct peaks and valleys indicating the effect of each frequency on the ability of the model to distinguish between SOC-balanced and SOC-imbalanced modules. Notably, clear peaks and troughs in the frequency spectrum are shown, with higher peaks indicating a stronger influence on the model's decision-making process. In particular, specific frequencies exhibit negative weights, suggesting that the features at these frequencies contribute inversely to the identification of SOC imbalances. The distribution of weights is relatively balanced for Re(Z) and Abs(Z). However, slight weight variations within this stable range suggest that different frequencies still significantly affect the model's decision process. On the other hand, a wider range of coefficient weights for the Im(Z) and Pha(Z) indicates a more pronounced variability. This variability indicates that the Im(Z) and Pha(Z) features within specific frequency ranges substantially differentiate the model's ability to detect SOC imbalances in the modules.

4.3.2. Scenario-2: SOH Imbalance

Following the SVM classification analysis used for SOC imbalances, a similar methodology is applied to investigate SOH imbalances. Module-level EIS measurements of Module-1 and Module-2 from Scenario-1 and Scenario-2 were classified as "SOH Balance," while the measurements of Module-3 in both scenarios were categorized as "SOH Imbalance." This classification aimed to distinguish between balanced versus imbalanced SOH within a module, regardless of the SOC. The dataset is randomly shuffled with a fixed state for reproducibility and divided into a training set (60% of data) and a test set (40% of data), as in Scenario-1.

As stated in **Table 5**, using the Re(Z), Im(Z), Abs(Z), or Pha(Z) as a fixed feature for classification resulted in the model achieving

Research Article
doi.org/10.1002/batt.202500284
Chemistry Europe
European Chemical Societies Publishing

Table 5. SVM classification results of the SOH imbalanced scenario based on impedance parameters.

Scenario	Modules	Precision	Recall	F1 Score
Scenario-2 (SOH Imbalanced Scenario)		Re(Z)		
	1 vs. 3	1	1	1
	2 vs. 3	1	1	1
	1 & 2 vs. 3	0.93	0.92	0.91
		Im(Z)		
	1 vs. 3	1	1	1
	2 vs. 3	1	1	1
	1 & 2 vs. 3	0.93	0.92	0.91
		Abs(Z)		
	1 vs. 3	1	1	1
	2 vs. 3	1	1	1
	1 & 2 vs. 3	1.00	1.00	1.00
		Pha(Z)		
	1 vs. 3	1	1	1
	2 vs. 3	1	1	1
	1 & 2 vs. 3	0.96	0.96	0.96

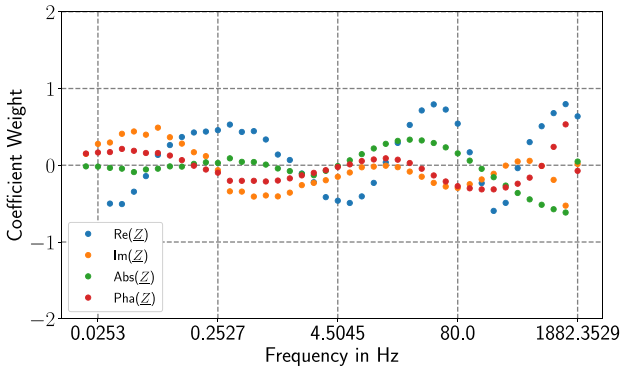

Figure 7. Coefficient weights of three modules (Modules 1&2 vs. 3) based on Scenario-2 using Re(Z), Im(Z), Abs(Z), or Pha(Z) as a feature.

a 100% accuracy in its predictions, emphasizing the relative ease of detecting SOH imbalances within these battery modules. However, the precision of the SVM model experienced a slight decline to 93% (with Re(Z) and Im(Z) and 96% (with Pha(Z) when the measurements of Module-1 and Module-2 were combined as the "SOH-balanced" class. This decline could be attributed to the limited size of the dataset.

While the classification results for SOH imbalances using Re(Z), Im(Z), Abs(Z), or Pha(Z) data achieved similar levels of accuracy, a closer look at **Figure 7** reveals distinct differences in how impedances at specific frequencies contribute to the SVM classification model's decision-making process. Each coefficient weight in the figure reflects its importance in the classification model for distinguishing between SOH-balanced modules (Module-1 and Module-2) and the SOH-imbalanced module (Module-3). Positive weights indicate that impedance characteristics at these frequencies have a positive influence on the SVM model's decision. In contrast, negative weights indicate that features at these frequencies have a negative influence on the model's decision. The distribution of weights for the Re(Z) feature indicates that all frequency ranges impact the model's decision. Nevertheless, the weights for Abs(Z), Im(Z), and Abs(Z) demonstrate significant variability, implying that these impedance characteristics at specific frequency points are more influential than others. This nonhomogeneous distribution of weights underscores the varying importance of impedance characteristics at different frequencies in detecting SOH imbalances with the SVM classification method.

4.4. Comparison of Analytical Methods

The strengths, limitations, and performance assessment of each analytical approach for detecting internal SOC and SOH imbalances in battery modules with series-connected cells through EIS are summarized in **Table 6**. The single-point impedance diagnostic method provides a quick and qualitative assessment by focusing on impedance changes at key frequencies. Its main limitation is ignoring broader impedance behaviors occurring over a wider frequency spectrum. The Pearson correlation analysis reveals correlations between impedance and imbalance over wide frequency ranges. It is particularly valuable for identifying consistent trends that are not visually apparent. However, this method is inherently limited to linear correlations. The SVM classification method handles both linear and nonlinear data. Its main drawback is requiring an extensive, well-labeled dataset. Their performances in imbalance detection are summarized below.

Table 6. Comparison of methods for the analysis of module-level EIS data.

Method	Strengths	Limitations	Performance in imbalance detection	
Single-point impedance diagnostic method	- Quick insights - Focuses on significant frequencies	- Overlooks broader impedance behavior	SOC imbalance detection	SOH imbalance detection
			- Difficulties with SOC imbalance detection in the fresh module	- Effective, especially at $f_{diffusion}$ at 5% and 100% SOC levels
Pearson correlation analysis	- Identifies broader trends - Comprehensive view	- Limited to linear correlations	- Provides low PCC values with the fresh module and high PCC values with the aged module	- Effective, with higher PCC values especially in the low- and medium-frequency ranges at 5% SOC
SVM classification	- High predictive accuracy - Handles nonlinear data	- Requires a large labeled dataset	- Low accuracy rate with three modules	- Effective with a very high accuracy rate

On the one hand, the detection of SOC imbalances at frequencies f_{ohmic} and $f_{diffusion}$ is challenging for the fresh module with single-point impedance diagnostics. This challenge is further highlighted by the low PCC values and SVM classification F1 scores, indicating the difficulty of SOC imbalance detection in fresh modules. Conversely, aged and mixed modules exhibited significant impedance variations across the SOC levels at two predetermined frequencies, demonstrating the clear impact of aging on SOC imbalance detection. The improved accuracy of the SVM model for these modules and higher PCC values of these modules confirm the relevance of the aging effect.

On the other hand, it is found that the imbalances in SOH are detectable at different SOC levels with single-point impedance diagnostics, especially at 5% and 100% SOCs. These observations are supported by the highest PCCs, particularly at 5% SOC and in the medium- and low-frequency ranges for almost all SOC values, emphasizing the crucial role of both SOC level and frequency region in identifying SOH imbalances. Furthermore, the performance of the SVM classification method for SOH imbalances is remarkable, and it achieves an accuracy of 100% when either the real or imaginary part of the impedance is used as a feature. This noteworthy accuracy emphasizes the effectiveness and relative ease of the method in detecting SOH imbalances in the modules.

Furthermore, in addition to working separately, these methods can synergistically enhance the detection of imbalances by utilizing the speed, broad scope, and predictive accuracy of their respective capabilities to provide a more thorough, comprehensive, and robust solution for battery diagnostics.

5. Conclusion

This paper has investigated SOC and SOH imbalances within battery modules with series-connected cells through module-level EIS measurements. The measurement results are analyzed using single-point impedance diagnostic, Pearson correlation analysis, and SVM classification methods. These methodologies have enhanced the detection and characterization of SOC and SOH imbalances in battery modules.

The findings indicate challenges in identifying SOC imbalances in fresh modules, whereas aged and mixed modules displayed significant impedance variations across all three methods. On the other hand, for SOH imbalance detection, single-point impedance diagnostic proves effective, especially at $f_{diffusion}$ at 5% and 100% SOCs. The Pearson correlation analysis highlights the importance of the medium-frequency range, while SVM classification demonstrates high accuracy using impedance data, underscoring its utility.

In summary, this study provides a comparative insight into various diagnostic techniques for detecting internal SOC and SOH imbalances, emphasizing the value of advanced analytical methods in enhancing battery module diagnostics and management. Furthermore, these methods can be integrated into an online BMS for real-time monitoring and diagnostics by automating key frequency monitoring and utilizing ML models to continuously assess SOC and SOH imbalances. These results are particularly relevant for the second-life utilization of battery packs from electric transportation to stationary energy storage systems, which require significant efforts in internal imbalance detection. We also acknowledge the evolving nature of the field, and ongoing research may uncover additional influencing factors for imbalance detection. Therefore, future investigation is encouraged to extend EIS at the module level for different cell chemistries, various scales, and operating conditions, paying particular attention to the influence of temperature, which was kept constant at 25 °C in this study.

Acknowledgements

The research was supported by the German Federal Ministry of Education and Research (BMBF) under the project OptiPro (Funding Code: 03XP0364A). The project DEAL enabled and organized open-access funding.

Open Access funding enabled and organized by Projekt DEAL.

Conflict of Interest

The authors declare no conflict of interest.

Data Availability Statement

The data that support the findings of this study are available from the corresponding author upon reasonable request.

Keywords: electrochemical impedance spectroscopy · imbalance detection · lithium-ion batteries · state of charge · state of health

[1] International Energy Agency, Batteries and Secure Energy Transitions, **2024**, https://www.iea.org/reports/batteries-and-secure-energy-transitions.
[2] W. Waag, C. Fleischer, D. U. Sauer, *J. Power Sources* **2014**, *258*, 321.
[3] J. Gallardo-Lozano, E. Romero-Cadaval, M. I. Milanes-Montero, M. A. Guerrero-Martinez, *J. Power Sources* **2015**, *299*, 356.
[4] S. Wang, J. Zhang, O. Gharbi, V. Vivier, M. Gao, M. E. Orazem, *Nat. Rev. Methods Primers* **2021**, *1*, 41.
[5] A. Blömeke, K. L. Quade, D. Jöst, W. Li, F. Ringbeck, D. U. Sauer, *Properties of a Lithium-Ion Battery as a Partner of Power Electronics, 2022 24th European Conference on Power Electronics and Applications (EPE'22 ECCE Europe)*, Hanover, Germany **2022**, 1–10.
[6] J. Xu, C. C. Mi, B. Cao, J. Cao, *J. Power Sources* **2013**, *233*, 277.
[7] J. G. Zhu, Z. C. Sun, X. Z. Wei, H. F. Dai, *J. Power Sources* **2015**, *274*, 990.
[8] F. Luo, H. Huang, L. Ni, T. Li, *J. Energy Storage* **2021**, *41*, 102866.
[9] K. Mc Carthy, H. Gullapalli, K. M. Ryan, T. Kennedy, *J. Energy Storage* **2022**, *50*, 104608.
[10] W. Waag, S. Käbitz, D. U. Sauer, *Applied Energy* **2013**, *102*, 885.
[11] L. Wang, X. Zhao, Z. Deng, L. Yang, *J. Energy Storage* **2023**, *57*, 106275.
[12] X. Wang, X. Wei, H. Dai, *J. Energy Storage* **2019**, *21*, 618.
[13] U. Westerhoff, T. Kroker, K. Kurbach, M. Kurrat, *J. Energy Storage* **2016**, *8*, 244.
[14] X. Du, J. Meng, J. Peng, Y. Zhang, T. Liu, R. Teodorescu, *IEEE Trans. Power Electron.* **2022**, *37*, 10101.
[15] Y. Zhang, Q. Tang, Y. Zhang, J. Wang, U. Stimming, A. A. Lee, *Nat. Commun.* **2020**, *11*, 1706.
[16] Z. Zhou, Y. Li, Q.-G. Wang, J. Yu, in *IEEE Transactions on Instrumentation and Measurement*, **2023**, *72*, pp. 1–1, https://doi.org/10.1109/TIM.2023.3272401.
[17] T. Rüther, C. Plank, M. Schamel, M. A. Danzer, *Appl. Energy* **2023**, *332*, 120514.

[18] M. Ank, J. Göhmann, M. Lienkamp, *Batteries* **2023**, *9*, 415.
[19] T. Yokoshima, D. Mukoyama, H. Nara, S. Maeda, K. Nakazawa, T. Momma, T. Osaka, *Electrochim. Acta* **2017**, *246*, 800.
[20] M. Kasper, M. Moertelmaier, M. Ragulskis, N. Al-Zubaidi R-Smith, J. Angerer, M. Aufreiter, A. Romero, J. Krummacher, J. Xu, D. E. Root, F. Kienberger, *Batteries Supercaps* **2023**, *6*, e202200415.
[21] S. Zhang, Z. Wei, L. Zhang, J. Hu, R. Dai, *J. Power Sources* **2024**, *600*, 234239.
[22] D. Kehl, T. Jennert, F. Lienesch, M. Kurrat, *Batteries* **2021**, *7*, 32.
[23] Y. Wang, H. Huang, H. Wang, *J. Energy Storage* **2023**, *63*, 107102.
[24] X. Li, L. Zhang, Y. Liu, A. Pan, Q. Liao, X. Yang, *Energy Res* **2020**, *44*, 2337.
[25] W. Zhang, R. Ahmed, S. Habibi, *in: 2023 IEEE Transportation Electrification Conference & Expo (ITEC)*, IEEE, Detroit, MI, USA **2023**, pp. 1–5.
[26] W. Yang, M. Lang, X. Yu, X. Yang, *J. Power Sources* **2024**, *593*, 233949.
[27] N. Togasaki, T. Yokoshima, Y. Oguma, T. Osaka, *J. Electrochem. Sci. Technol* **2021**, *12*, 415.
[28] G. Caposciutti, G. Bandini, M. Marracci, A. Buffi, B. Tellini, in: 2021 IEEE International Workshop on Metrology for Automotive (MetroAutomotive), Bologna, Italy **2021**, pp. 36-41, https://doi.org/10.1109/MetroAutomotive50197.2021.9502724.
[29] B. M. Huhman, J. M. Heinzel, L. Mili, C. T. Love, D. A. Wetz, *J. Electrochem. Soc.* **2017**, *164*, A6401.
[30] C. T. Love, M. B. V. Virji, R. E. Rocheleau, K. E. Swider-Lyons, *J. Power Sources* **2014**, *266*, 512.
[31] R. R. Richardson, P. T. Ireland, D. A. Howey, *J. Power Sources* **2014**, *265*, 254.
[32] N. S. Spinner, C. T. Love, S. L. Rose-Pehrsson, S. G. Tuttle, *Electrochim. Acta* **2015**, *174*, 488.
[33] C. Love, M. Dubarry, T. Reshetenko, A. Devie, N. Spinner, K. Swider-Lyons, R. Rocheleau, *Energies* **2018**, *11*, 834.
[34] X. Gu, K. W. See, Y. Liu, B. Arshad, L. Zhao, Y. Wang, *J. Power Sources* **2023**, *581*, 233472.
[35] I. Babaeiyazdi, A. Rezaei-Zare, S. Shokrzadeh, *Energy* **2021**, *223*, 120116.
[36] M. Faraji-Niri, M. Rashid, J. Sansom, M. Sheikh, D. Widanage, J. Marco, *J. Energy Storage* **2023**, *58*, 106295.
[37] W. Luo, A. U. Syed, J. R. Nicholls, S. Gray, *J. Electrochem. Soc.* **2023**, *170*, 030532.
[38] V. M. Nagulapati, S. S. Kumar, V. Annadurai, H. Lim, *Energy AI* **2023**, *12*, 100237.
[39] J. Zhang, A. T. Gao, R. G. Chen, Y. S. Han, *AMR* **2013**, *724–725*, 797.
[40] Y. Li, M. Maleki, S. Banitaan, M. Chen, *State of Health Indicator Modeling of Lithium-ion Batteries Using Machine Learning Techniques, in: 2022 IEEE Inter. Conf. on Electro Information Technology (eIT)*, IEEE, Mankato, MN, USA, **2022**, pp. 440–445.
[41] U. Westerhoff, K. Kurbach, F. Lienesch, M. Kurrat, *Energy Technol.* **2016**, *4*, 1620.
[42] P. Iurilli, C. Brivio, V. Wood, *J. Power Sources* **2021**, *505*, 229860.
[43] N. Gogtay, U. Thatte, *J. Assoc. Physicians India* **2017**, *65*, 78.
[44] Q. Gu, L. Zhu, Z. Cai, *Computational Intelligence And Intelligent Systems*, (Eds: Z. Cai, Z. Li, Z. Kang, Y. Liu), Springer Berlin Heidelberg, Berlin, Heidelberg **2009**, pp. 461–471.
[45] L. Wildfeuer, M. Lienkamp, *eTransportation* **2021**, *9*, 100129.
[46] M. Schönleber, D. Klotz, E. Ivers-Tiffée, *The Lin-KK Tool – Kramers-Kronig Validity Test Lin-KK for Impedance Spectra*, Karlsruhe Institute of Technology (KIT), Karlsruhe (Germany), (n.d.), can be found under https://www.iam.kit.edu/et/english/Lin-KK.php (Accessed: July, 2025).
[47] B. A. Boukamp, *J. Electrochem. Soc.* **1995**, *142*, 1885.
[48] M. Schönleber, D. Klotz, E. Ivers-Tiffée, *Electrochim. Acta* **2014**, *131*, 20.
[49] Y. Xie, J. Kim, M. Lee, J. Park, W. Na, *J. Electrochem. Soc.* **2021**, *168*, 090548.
[50] P. Shafiei Sabet, G. Stahl, D. U. Sauer, *J. Power Sources* **2020**, *472*, 228189.
[51] D. Wong, B. Shrestha, D. A. Wetz, J. M. Heinzel, *J. Power Sources* **2015**, *280*, 363.
[52] Y. Zhang, C.-Y. Wang, *J. Electrochem. Soc.* **2009**, *156*, A527.

Manuscript received: April 15, 2025
Revised manuscript received: June 20, 2025
Version of record online: